Radiation Fields of a Tapered Film and a Novel Film-to-Fiber Coupler

P. K. TIEN, FELLOW, IEEE, GERALD SMOLINSKY, AND R. J. MARTIN

(*Invited Paper*)

***Abstract*—Light in a tapered thin-film optical waveguide radiates into the substrate because the waveguide mode in the taper becomes cut off. Our measurement of the radiation pattern shows that the light emerges from the taper as a narrow beam with an angular width of only 2°–4°. We have studied the problem based on ray optics and based on a wave theory of radiation modes. We also have demonstrated a film-to-fiber coupler in which an optical fiber collects all the light emerging from the taper.**

I. INTRODUCTION

IN an earlier paper [1] we described a tapered-film light-wave coupler which consisted of a thin zinc-sulfide film with a tapered edge deposited on a glass substrate. Fig. 1 schematically represents two experiments described in that paper. In the first, a light wave propagating in the film enters the substrate via the taper and appears as a narrow beam of light in the substrate. In the second, a laser beam in space is focused on the substrate in the direction toward the taper and is coupled into the film via the taper. It is evident from these two experiments that a tapered film can convert light in a film in a waveguide mode into radiation fields in a substrate and vice versa. It is also evident that a light wave propagating in a tapered film will reach a point where the film is so thin that the waveguide becomes cut off. Beyond this cutoff point (C in Fig. 1) the waveguide mode no longer exists and all the light in the film is converted into radiation fields. Therefore, a tapered-film coupler critically involves the cutoff property of an optical waveguide.

This earlier study posed several intriguing questions. Why does the radiation field in the substrate appear as a well-defined light beam at an angle several degrees below the film–substrate interface? How does the radiation pattern vary with the slope of the taper? Can all the radiation in the substrate be collected by an optical fiber to form a film-to-fiber coupler?

We have measured the radiation patterns of tapered films and made confirmatory calculations using a very simple ray-optics analysis. In addition, we have formulated a wave theory of radiation fields based on work by Marcuse [2] and will discuss its salient features. We also will describe a prototype film-to-fiber coupler which is more than 95-percent efficient in coupling light from the film to the fiber. The advantage of this coupler is that it leaves the surface of the waveguide film untouched.

Manuscript received April 2, 1974; revised July 15, 1974.

P. K. Tien and R. J. Martin are with Bell Laboratories, Holmdel, N. J. 07733.

G. Smolinsky is with Bell Laboratories, Murray Hill, N. J. 07974.

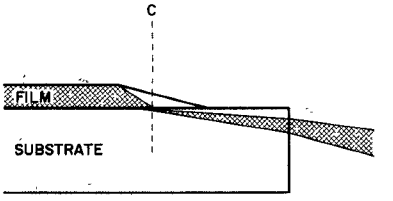

Fig. 1. Schematic representation of a tapered thin film on a substrate with a light beam passing from the film into the substrate and projecting from the substrate.

II. RADIATION FIELDS AND RAY OPTICS

A more rigorous theory of radiation fields will be given in Sections V and VI of this paper. For the moment, it is instructive to consider the problem rather crudely using a ray-optics analysis. Ray optics has been used successfully in depicting light waves in optical waveguides of planar geometry. It is also used extensively for imaging approximating what is essentially a far-field calculation. We therefore are not surprised to find good agreement between the radiation pattern calculated by ray analysis and the experiment.

Fig. 2 depicts a zigzag TE wave [4] propagating in a film with a 30:1 taper. The film was prepared from vinyltrimethylsilane (VTMS) [3] on a plexiglass substrate with refractive indices at 0.6328 μm of n_1 (film) = 1.5327 and n_0 (substrate) = 1.4876, respectively. As the wave propagates through the taper, the angle between the zigzag ray and the normal of the film–substrate interface becomes smaller and smaller. Eventually, at $x = a'$, the incident angle θ_I equals the critical angle θ_c. From this point on, the optical ray is partially reflected by the film and partially refracted into the substrate. Note that ray optics gives the value for the critical angle as

$$\theta_c = \sin^{-1}(n_0/n_1) = 76° 07',$$

and the corresponding mode index as $\beta/k = n_1 \sin\theta_c = n_0$. The latter is precisely the condition of cutoff in the wave theory of waveguide modes. From the wave theory, we

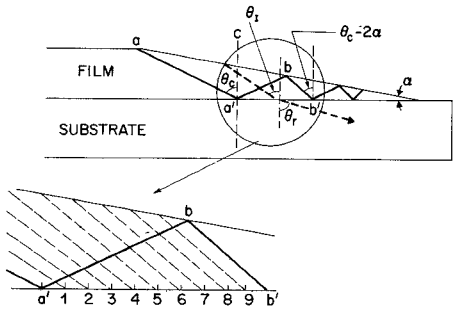

Fig. 2. Schematic representation of a zigzag TE wave propagating in a 30:1 tapered thin-film waveguide.

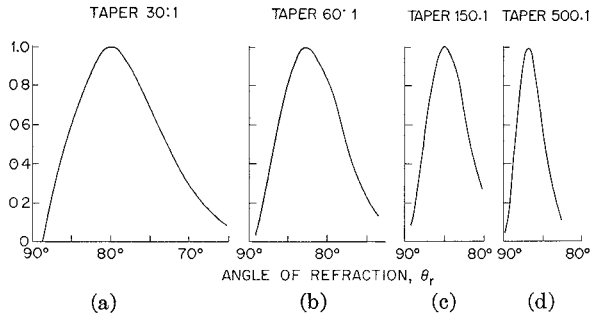

Fig. 3. Computed normalized intensity I_θ of the radiation patterns for a TE_0-mode wave as a function of angle of refraction θ_r in the following tapers. (a) 30:1. (b) 60:1. (c) 150:1. (d) 500:1.

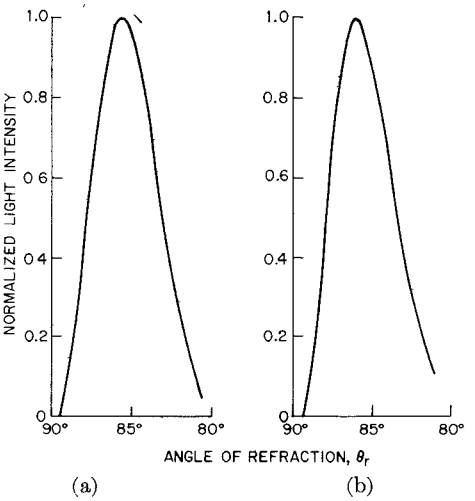

Fig. 4. Computed normalized intensity I_θ of the radiation pattern for (a) the TE_0 and (b) the TE_1 modes as a function of angle of refraction θ_r in a 250:1 taper.

found that at cutoff of the $m = 0$ mode the thickness of the VTMS film is $W = 0.354$ μm.

Let a–a' in Fig. 2 be a ray of the zigzag wave which has an incident angle $\theta_I = \theta_c$ at the cutoff point a'. After another zigazg, the wave reaches point b' where $\theta_I = \theta_c - 2\alpha$, α being the angle of the taper. Now let us fill the space between a' and b' by $(N - 1)$ equally spaced rays, 1,2,3,$\cdots$. These rays have incident angles $I_I = \theta_c - (2\alpha/N)$, $\theta_I = \theta_c - (4\alpha/N)$, $\theta_I = \theta_c - (6\alpha/N)$,$\cdots$ at points 1,2,3,$\cdots$, respectively. The angle of refraction θ_r at each of these points can be computed from the incident angle θ_I by the Snell [5] law of refraction. From the waveguide theory [4], the relationship of the power P_I in the waveguide to the electric-field amplitude E_{yI} in the film is given by

$$P_I = (1/\omega\mu)kn_1 \sin\theta_I E_{yI}^2(W + 1/p_2) \qquad (1)$$

where W is the film thickness and $(1/p_2)$ is the distance that the fields penetrate into the air space. The quantities, ω and μ are, respectively, the laser angular frequency and the magnetic permeability of the film. We used MKS units and have purposely ignored the fringing fields in the substrate since we treat the fields at the film–substrate interface by ray optics. The power P_r refracted into the substrate along the interface at distances Δx between any two neighboring points, such as 2 and 3, is related to the electric field E_{yr} in the substrate by

$$P_r = (1/2\omega\mu)kn_0\Delta x \cos\theta_r E_{yr}^2. \qquad (2)$$

Finally, E_{yr} at each of the points 1,2,3,$\cdots$ can be computed from E_{yI} at that point by the usual Fresnel [5, pp. 38–39] formula of refraction.

At this stage of our analysis, we must reconcile ray optics with the wave picture. In Fig. 2 the wave propagates from left to right and the power in the film at point 1 must be equal to that at point a' minus the portion refracted into the substrate through the space $a' - 1$. Similarly, the power in the film at point 2 is that at point a' minus the sum of the portions refracted into the substrate through the spaces a'–1 and 1–2, and so on. The required calculation can be summarized as follows: Knowing the power P_{I1} in the waveguide at point 1, we calculate E_{yI1} using (1) and determine E_{yr1} from E_{yI1} with the Fresnel formula. Next, the power P_{r1} refracted into the substrate through the space 1–2 is computed from E_{yr1} with (2). Finally, the power in the film at point 2 is $P_{I2} = P_{I1} - P_{r1}$. We then repeat the same series of computations for point 2, and so on.

Despite the simplicity of the analysis, the use of ray optics gives all answers qualitatively correct. The calculated radiation pattern concides with the experiment; a narrow beam of light propagating at an angle several degrees below the film–substrate interface. Fig. 3(a)–(d) shows the intensity of the radiation I_θ as a function of angle of refraction θ_r. To be specific, I_θ is the normalized radiation intensity per unit angle such as I_θ at point 2 is $P_{r2}/(\theta_{r3} - \theta_{r2})$. At the cutoff point, $\theta_r = 90°$ (the grazing angle) and I_θ is zero because the light is still totally reflected at the film–substrate interface. As the wave propagates beyond this point, both θ_I and θ_r decrease. At first, I_θ increases because the reflectance at the interface decreases rapidly and more power is refracted into the substrate, but after passing through a maximum, I_θ quickly falls off to zero as the power in the film is depleted. Fig. 3 also shows that a longer taper has a narrower radiation pattern, which agrees with the measurements described in the next section.

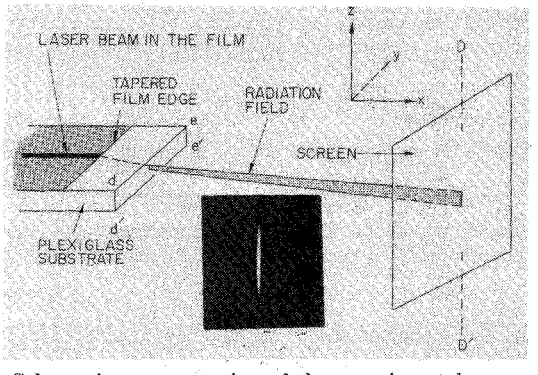

Fig. 5. Schematic representation of the experimental arrangement used to measure the radiation fields in the tapered films.

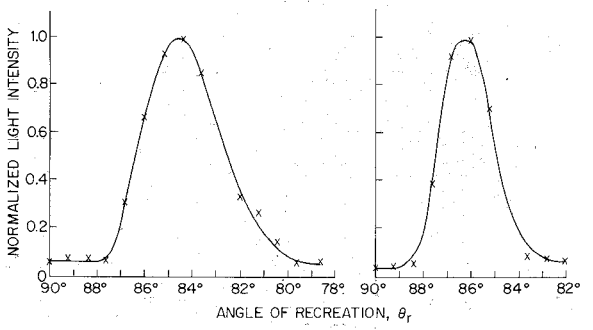

Fig. 6. Measured normalized intensity I_θ of the radiation pattern for a TE_0-mode light wave as a function of angle of refraction θ_r in a (a) 120:1 taper and (b) 300:1 taper film of thicknesses 0.6 and 0.65 μm, respectively.

Fig. 4(a) and (b) shows the calculated radiation patterns of the $m = 0$ and $m = 1$ TE waveguide modes for a taper of 300:1. The radiation patterns are seen to be almost identical, again in fair agreement with the experiment as discussed in the next section.

III. MEASUREMENT OF THE RADIATION FIELDS

An experimental arrangement illustrated in Fig. 5 was used to measure the radiation fields. A tapered VTMS film [7] was deposited on a plexiglass substrate so that the tapered edge was parallel to the substrate end *de* and 5 mm away from it. The substrate output surface *dee'd'* was well polished. A light wave from a 0.6328-μm helium–neon laser was excited in the VTMS film by a prism coupler. The light wave then entered the substrate after reaching the tapered edge and finally projected through the output surface to a screen which was located a distance of 9.7 cm from the taper. A typical far-field image of the radiation observed on the screen is shown in the insert of Fig. 5. The width of the image (parallel to the y direction) is controllable and depends on the width of the light beam in the film. The vertical height of the image (parallel to the z direction) depends only on the slope of the taper. In order to measure the radiation-field pattern,

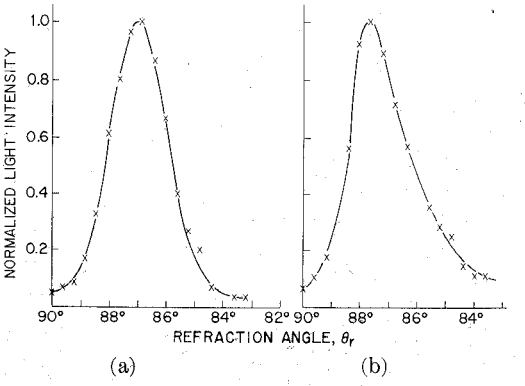

Fig. 7. Measured normalized intensity I_θ of the radiation pattern for the (a) TE_0 and (b) TE_1 modes as a function of angle of refraction θ_r in a 300:1 taper for a 1.2-μm-thick film.

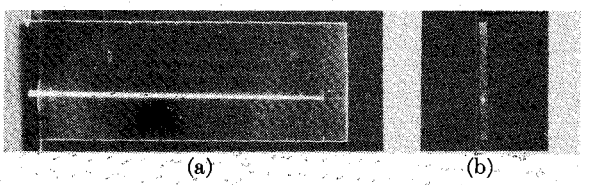

Fig. 8. Photographs of (a) a light streak propagating in a thin-film waveguide from left to right and radiating into the substrate at the tapered edge, and (b) the light-beam spot at the polished end of the substrate.

we replaced the screen by a pinhole detector and measured the intensity of the field by moving the detector along the line DD'. The pinhole was large enough to cover the entire width of the image. Each position of the detector along the line DD' corresponds to an angle of refraction θ_r inside the substrate. By plotting the measured light intensity versus θ_r, we obtained the radiation pattern shown in Figs. 6 and 7. We estimated the error in the measurement to be about 2 percent. The dimensions of the tapers were determined with a Leitz interference microscope [7]. Because the tapers were not linear and because it was impossible to determine the exact position of the cutoff point, we used the average slope of the taper as its slope at the cutoff point.

Fig. 6(a) and (b) shows the measured radiation patterns for 120:1 and 300:1 tapers, respectively, in about a 0.6-μm-thick film. These curves should be compared with the ray-optics calculated curves in Fig. 3(c) and (d). Although the calculated radiation patterns are somewhat wider, the agreement is good in view of the crudeness of the theory. Fig. 7(a) and (b) is the measured radiation patterns for the $m = 0$ and $m = 1$ modes, respectively, in a 300:1 taper in a 1.2-μm-thick film. These curves should be compared with those in Fig. 4(a) and (b) of Section II.

Fig. 8(a) is a photograph showing a bright streak of light propagating in a film up to the tapered edge. Since the observed light is due mainly to surface scattering, the light beam appears as a fine line while it is inside the

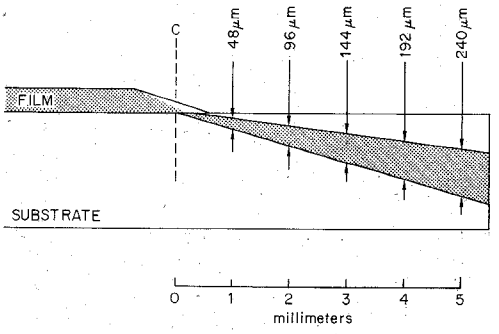

Fig. 9. Schematic representation of the profile of the radiation wave in the substrate as calculated from the experimental-field pattern curve of Fig. 7(b).

bulk of the substrate. Fig. 8(b) is a photograph taken of the output surface *dee'd'* (Fig. 5) of the substrate and shows a well-defined beam spot below the film–substrate interface. In order to avoid directional effects of the light beam, this photograph was taken with a diffused screen placed against the output substrate surface.

IV. A FILM-TO-FIBER COUPLER

We have constructed a film-to-fiber coupler which takes advantage of the fact that a light beam in its waveguide mode in a tapered thin film is completely coupled into the supporting substrate by the taper as radiation modes. Now to make an efficient film-to-fiber coupler, all the radiation in the substrate must be intercepted by the optical fiber. Fig. 9 helps make clear the nature of the problem of interception. This figure shows an exaggerated drawing of the calculated radiation profile using the experimental far-field-pattern data of Fig. 7(b). The profile has the approximate cross sections of 48, 96, 144, 192, and 240 μm at distances from the cutoff point of 1, 2, 3, 4, and 5 mm, respectively. In order to intercept the beam with a 50-μm-core-diam fiber, for example, it would be necessary to place the end of the fiber within a distance of 1 mm from the taper. However, at such a short distance from the taper, the beam is only about 50 μm below the film–substrate interface, thus making it very difficult to use fibers having very small core diameters.

To demonstrate the principle, we used a fiber having a core diameter of 275 μm, which could intercept all the light at a distance of about 5 mm from the taper. The fiber core was made of Suprasil-2 glass with a Dupont FEP 100 cladding having refractive indices of 1.458 and 1.338, respectively. A VTMS film with a 300:1 taper, possessing the intensity profile shown in Fig. 7(b), was deposited on a plexiglass substrate [3] with the taper 5 mm from the polished end of the substrate, as depicted in Fig. 5. The cladding was stripped back a short distance from a square-cut end of the fiber, and the fiber end placed over the bright spot of light projecting from the substrate surface, *dee'd'* in Fig. 5. A photograph of the coupling, which was 75-percent efficient, is shown in Fig. 10(a). By wetting the fiber end with a drop of liquid ($n = 1.51$) and repeating the procedure, a coupling efficiency of more than 95 percent

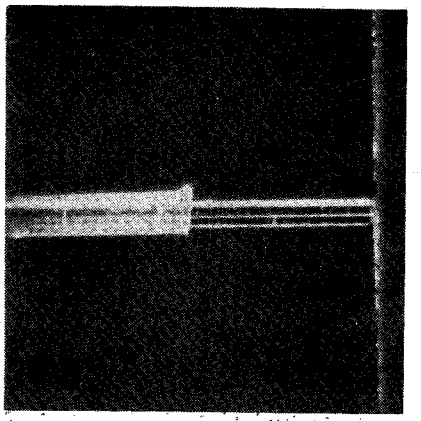

(a)

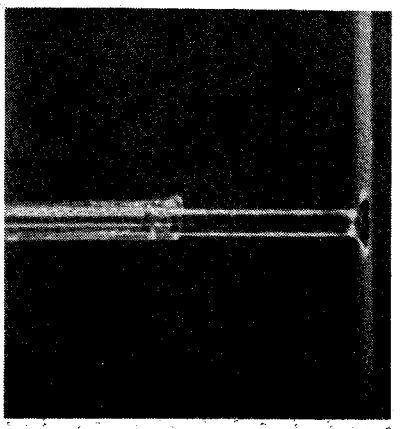

(b)

Fig. 10. Photographs of a fiber intercepting a light beam from the polished surface of a plexiglass substrate.

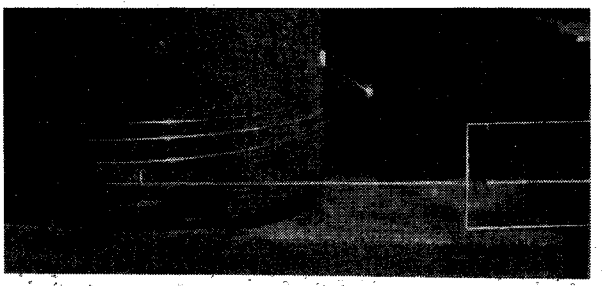

Fig. 11. Photograph of a film-to-fiber coupler.

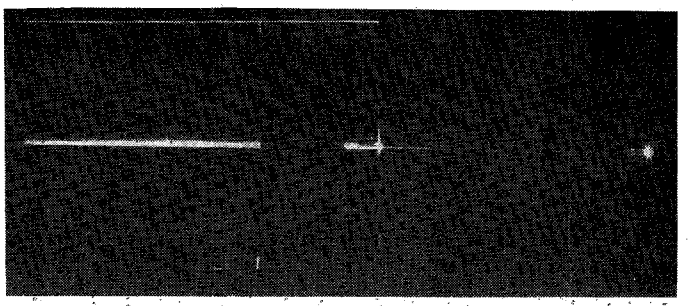

Fig. 12. Photograph of a film-to-fiber coupler consisting of an optical fiber held firmly in a hole drilled in the substrate below the film–substrate interface several millimeters from the end of the tapered film edge.

was achieved [Fig. 10(b)]. A photograph of the entire film-fiber coupler is shown in Fig. 11.

Similar results have also been obtained using a slightly different arrangement, as shown in Fig. 12. Here a slanting hole with a hemispherical end was drilled into the substrate surface *dee'd'* (Fig. 5) ending just below the film–substrate interface. A tapered film was deposited on the substrate so that the taper was but a few millimeters from the hole. An optical fiber was carefully inserted into the hole which was then filled with an index-matching liquid. Using a liquid of refractive index higher than that of the substrate, the hemispherical end of the hole formed a converging lens which further improved the optics. We foresee that slight modification of this latter arrangement could result in the fiber being firmly bound in the hole to the substrate, resulting in a practical coupler.

It is likely that multimode fibers will be used in the future optical-communication systems. Because of the use of the multimode fiber, the problems associated with the coupling from a fiber to film are in some important ways different from those associated with the coupling from a film to fiber. We have seen that the radiation pattern of a tapered film is a narrow beam of light which is rather simple to focus on the end of an optical fiber. On the other hand, the radiation pattern from the end of a multimode fiber varies considerably, depending on how the light wave is excited in the fiber. Thus the construction of a fiber-to-film coupler appears to be a more difficult problem, very likely requiring a different experimental approach.

V. A WAVE ANALYSIS OF A TAPERED FILM

An elegant theory of radiation modes in a planar optical waveguide has been formulated by Marcuse [2]. He used his theory to study radiation losses in a tapered symmetric dielectric-slab waveguide [2]. Here we will consider the more complex case of an asymmetric optical waveguide. An asymmetric waveguide [4] involves discrete waveguide modes and continuous substrate and air modes. The mode indices [4] of the waveguide modes range from n_0 to n_1, those of the substrate from 1 to n_0, and of air from 0 to 1. The purpose of this section is to calculate the intensity distribution of the substrate modes as light in the film in a waveguide mode passes into the substrate as radiation modes.

The following assumptions were made for the purpose of simplification. First, we assumed the film has only one TE waveguide mode, obviating the need to consider coupling between different waveguide modes. This assumption is reasonable because near the cutoff, power conversion between waveguide modes is much less than power conversion between waveguide and substrate modes. For the same reason we can neglect completely the air modes. Next, we ignore the backward-traveling waves, since they never have been observed in any of our experiments. Finally, we ignore power conversion between substrate modes because these will be only small second-order quantities. In short, we will analyze as a first-order approximation the coupling of power from a forward-traveling light wave in a single TE waveguide mode to all possible forward-traveling substrate modes.

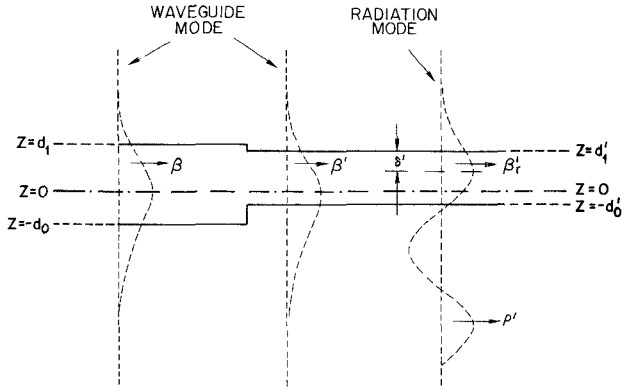

Fig. 13. A schematic representation of the waveguide and radiation modes traveling in a small-stepped thin-film waveguide.

We treated a long taper as if it were constructed of a very large number of small steps. A typical small step is shown in Fig. 13. As a light wave in a waveguide mode propagates through the step, part of it is converted into substrate modes while the remainder continues to propagate forward in the original waveguide mode. At the step, the newly converted light in each of the substrate modes adds vectorially to any previously converted light, and the combined light in all the substrate modes also continues to travel forward. Therefore, as the light travels from left to right in Fig. 13 through many, many steps of decreasing thickness, power in the radiation modes rises steadily at the expense of the waveguide mode until all the light in the waveguide is depleted.

For our mathematical symbolization, we will use the English letters b, p_0, and p_2 for the waveguide mode and the Greek letters σ, ρ, and γ for the substrate modes. The waveguide mode propagates as $\exp(-i\omega t + i\beta x)$ and the substrate modes as $\exp(-i\omega t + i\beta_r x)$. All the quantities belonging to the waveguide mode vary with x while those belonging to the substrate modes vary not only with x but in addition are different for different substrate modes. In Fig. 13, the upper and lower film surfaces are at the left of the step $z = d_1$ and $z = -d_0$, respectively, and at the right $z = d_1'$ and $z = -d_0'$, respectively.

Ignoring the common factor $\exp(-i\omega t + i\beta x)$, the field distribution of a TE waveguide mode is given by

$$\left.\begin{aligned} E_y &= AC(x)\cos bz, && -d_0 < z < d_1 \\ &= AC(x)\cos bd_1 \exp[-p_2(z-d_1)], && z > d_1 \\ &= AC(x)\cos bd_0 \exp[p_0(z+d_0)], && z < -d_0 \end{aligned}\right\} \tag{3}$$

where $C(x)C^*(x)$ is the power carried in the waveguide mode at x. The value of the power is equal to P at $x = -\infty$ and gradually decreases to zero as the wave approaches

the cutoff point, $x = C$. The other quantities in (3) are

$$A^2 = \frac{4\omega\mu}{\beta(d_1 + d_0 + 1/p_2 + 1/p_0)} \tag{4}$$

$$b^2 = k^2n_1^2 - \beta^2 \tag{5}$$

$$p_2^2 = \beta^2 - k^2n_2^2 \tag{6}$$

$$p_0^2 = \beta^2 - k^2n_0^2 \tag{7}$$

$$k = 2\pi/\lambda_0 \tag{8}$$

and ω and λ_0 are, respectively, the angular frequency and vacuum wavelength of the laser light.

Again ignoring the common factor $\exp(-i\omega t + i\beta_r x)$, the field distribution of a substrate mode is given by

$$\left.\begin{aligned} E_y &= BQ(x,\rho)\cos[\sigma(z-\delta)], && -d_0 < z < d_1 \\ &= BQ(x,\rho)\cos[\sigma(d_1-\delta)]\exp[-\gamma(z-d_1)], && z > d_1 \\ &= BQ(x,\rho)\exp[-i\rho(z+d_0)] \\ &\quad \cdot \{\cos[\sigma(d_0+\delta)] + i(\sigma/\rho)\sin[\sigma(d_0+\delta)]\} \\ &\quad + \text{complex conjugate}, && z < -d_0 \end{aligned}\right\} \tag{9}$$

where $Q(x,\rho)Q^*(x,\rho)\,d\rho$ is the power carried by the substrate mode ρ at x. Here we must distinguish a different ρ for each substrate mode. The other quantities in (9) are

$$B^2 = \frac{4\omega\mu}{\pi\beta_r[\cos^2\sigma(d_0+\delta) + (\sigma^2/\rho^2)\sin^2\sigma(d_0+\delta)]} \tag{10}$$

$$\sigma^2 = k^2n_1^2 - \beta_r^2 \tag{11}$$

$$\rho^2 = k^2n_0^2 - \beta_r^2 \tag{12}$$

$$\gamma^2 = \beta_r^2 - k^2n_2^2 \tag{13}$$

and

$$\delta = d_1 - \frac{1}{\sigma}\tan^{-1}(\gamma/\rho). \tag{14}$$

Now let the step shown in Fig. 13 be at $x = x'$; a certain fraction of the light in the waveguide mode is converted into a substrate mode ρ at this step. It can be easily shown that the converted quantity of light is $q(x',\rho)q^*(x',\rho)\,dx'\,d\rho$, where

$$\begin{aligned} q(x',\rho) &= \frac{1}{2\omega\mu}AC(x)B\frac{\beta_r}{\beta^2-\beta_r^2} \\ &\quad \cdot \{k^2(n_1^2-1)(d_1-d_1')\cos bd_1\cos[\sigma(d_1'-\delta)] \\ &\quad + k^2(n_1^2-n_0^2)(d_0-d_0')\cos bd_0 \\ &\quad \cdot \cos[\sigma(d_0'+\delta)]\}. \end{aligned} \tag{15}$$

From (9) and (15) we have at any x

$$Q(x,\rho) = \int_{-\infty}^{x} q(x',\rho)\exp\left[\int_{x'}^{x}\beta_r\,dx\right]dx'. \tag{16}$$

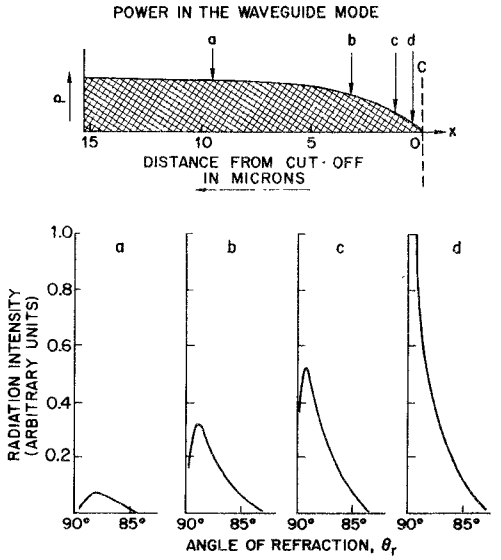

Fig. 14. Relationship of the power in the waveguide mode and the intensity of the radiation fields near the cutoff point C as a function distance before C for a 250:1 taper.

Consequently, the power carried in all the substrate modes at x is

$$P_r(x) = \int_{k(n_0^2-1)^{1/2}}^{0} Q(x,\rho)Q^*(x,\rho)\,d\rho \tag{17}$$

and at the same x the power remaining in the waveguide mode is

$$P(x) = 1 - P_r(x). \tag{18}$$

The previous calculation has been carried out with a digital computer for a 250:1 taper and a TE $m = 0$ mode. The results of the corresponding calculation based on ray optics has been shown earlier in Fig. 4(a). The results of this wave analysis will be discussed fully in the next section.

VI. DISCUSSION OF THE WAVE ANALYSIS

There are fundamental differences between the ray-optics (Section II) and wave (Section V) analysis. For example, in the former the wave is refracted into the substrate *after* reaching the cutoff point, whereas in the latter the wave is completely converted into the substrate modes *before* the cutoff point. However, both theories say that the conversion takes place within a distance of less than 20 μm of the cutoff point and that the light emerging from the taper into the substrate is a narrow beam.

In the wave analysis, as shown by (9), each substrate mode can be considered as a plane wave emerging from the film–substrate interface at an angle of refraction given by

$$\theta_r = \cos^{-1}(\rho/kn_0). \tag{19}$$

Therefore, by plotting the intensities of the substrate modes versus the corresponding calculated value of θ_r using (19), we again obtain a radiation pattern of the tapered film. In Fig. 14 we observed how the radiation fields in the substrate steadily build up as a light wave in the waveguide gradually approaches the cutoff point

C for a 250:1 taper. At point a, about 10 μm before C, the top diagram in Fig. 14 shows that the waveguide mode still retains 94 percent of the original intensity, while the lower left diagram shows the intensity distribution of the radiation at point a. At point b, about 3 μm from cutoff, 67 percent of the original power remains in the waveguide mode. At closer approaches to cutoff, points c and d, the power in the waveguide mode rapidly drains out. Correspondingly, we observe in the lower diagrams of Fig. 14 a sharp rise in the radiation intensity from point b to c to d.

At point d, the intensity distribution of the radiation is peaked at the grazing angle $\theta_r = 90°$, which agrees neither with experimental observation nor with the ray analysis. The difficulty involved here is the factor $1/(\beta^2 - \beta_r^2)$ in (15), which enhances the coupling to the substrate modes with $\theta_r \cong 90°$ as β approaches kn_0. In reality, as power is converted from the waveguide mode to radiation modes, β of the waveguide mode should be a complex number instead of the real number used in the present calculation. A more elaborate wave analysis involving complex propagation constants and including losses of the film is being studied.

VII. CONCLUSIONS

We have measured the radiation patterns of tapered thin-film optical waveguides. The radiation emerges from a certain point in the taper where the waveguide mode becomes cutoff and appears as a narrow beam of light inside the substrate. The half-intensity angular width of the radiation is 3.8° for a 120:1 taper, and is reduced to only 2.5° for a 300:1 taper; the radiation intensity peaks are at about 5° and 3.5°, respectively. For a given taper, different waveguide modes have nearly the same radiation pattern. We were able to explain all these phenomena by a simple ray-optics analysis, though the calculated radiation patterns were slightly wider than those observed experimentally. We also have studied the problem using a more rigorous wave analysis. Although we obtained a correct width for the radiation pattern, the intensity distribution was incorrect, indicating the needs for a more elaborate wave analysis with complex propagation constants.

By collecting the radiation in the substrate with an optical fiber, we have constructed a novel film-to-fiber coupler. This coupler has the advantage that the surface of the waveguide film is untouched and is left free for the fabrication of an integrated optical circuit. Because the radiation from a tapered film is very close to the film–substrate interface, construction of this type of coupler may be difficult for use with fibers having core diameters of less than 50 μm.

ACKNOWLEDGMENT

The authors wish to thank L. L. Blyler and A. C. Hart for supplying the optical fibers used in these experiments, some of which were fabricated according to our specifications.

REFERENCES

[1] P. K. Tien and R. J. Martin, *Appl. Phys. Lett.*, vol. 18, p. 398, 1971.
[2] D. Marcuse, *Bell Syst. Tech. J.*, vol. 48, p. 3187, 1969; also *Bell Syst. Tech. J.*, vol. 49, p. 273, 1970.
[3] P. K. Tien, G. Smolinsky, and R. J. Martin, *Appl. Opt.*, vol. 11, p. 638, 1972.
[4] P. K. Tien, *Appl. Opt.*, vol. 10, p. 2395, 1971.
[5] M. Born and E. Wolf, *Principles of Optics*. New York: Pergamon, 1959, p. 37.
[6] P. K. Tien, R. J. Martin, and G. Smolinsky, *Appl. Opt.*, vol. 12, p. 1909, 1973.

Tapered Optical Directional Coupler

MICHAEL G. F. WILSON AND G. A. TEH

***Abstract*—Tapered velocity optical directional couplers showing 100-percent coupling have been fabricated in thin film form. A computer analysis shows that this type of coupler has greatly improved tolerance properties and does not, in particular, suffer from the severe tolerance restriction placed on velocity synchronism in conventional uniform couplers.**

Manuscript received April 2, 1974; revised June 17, 1974. This work was supported by the Science Research Council.

The authors are with the Department of Electronic and Electrical Engineering, University College, London, England.

I. INTRODUCTION

THE AIM of current research in integrated optics is to develop a wide range of miniature optical components which will provide the means of generating, controlling, and detecting optical signals. The directional coupler is one such passive component which is a basic element in any waveguide system and which has direct application to multiplexing and modulation. Many designs of coupler are possible and in principle these may be developed from